

Hybrid Modeling of Evapotranspiration: Inferring Stomatal and Aerodynamic Resistances Using Combined Physics-Based and Machine Learning

Reda ElGhawi^{*1,2,3}, Basil Kraft¹, Christian Reimers¹, Markus Reichstein¹, Marco Körner³, Pierre Gentine⁴ and Alexander J. Winkler^{*1}

¹ Max Planck Institute for Biogeochemistry, Biogeochemical Integration, Jena, Germany

² International Max Planck Research School for Global Biogeochemical Cycles, Max Planck Institute for Biogeochemistry, Jena, Germany

³ Technical University of Munich, TUM School of Engineering and Design, Department of Aerospace and Geodesy, Munich, Germany

⁴ Department of Earth and Environmental Engineering, Columbia University, New York, NY, 10027, USA

* Authors to whom any correspondence should be addressed

E-mail: {relghawi, awinkler}@bgc-jena.mpg.de

Received xxxxxx; Accepted for publication xxxxxx; Published xxxxxx

Abstract

The process of evapotranspiration transfers water vapour from vegetation and soil surfaces to the atmosphere, the so-called latent heat flux (Q_{LE}), and thus crucially modulates Earth's energy, water, and carbon cycles. Vegetation controls Q_{LE} through regulating the leaf stomata (i.e., surface resistance r_s) and through altering surface roughness (aerodynamic resistance r_a). Estimating r_s and r_a across different vegetation types proves to be a key challenge in predicting Q_{LE} . Here, we propose a hybrid modeling approach (i.e., combining mechanistic modeling and machine learning) for Q_{LE} where neural networks independently learn the resistances from observations as intermediate variables. In our hybrid modeling setup, we make use of the Penman-Monteith equation based on the Big Leaf theory in conjunction with multi-year flux measurements across different forest and grassland sites from the FLUXNET database. We follow two conceptually different strategies to constrain the hybrid model to control for equifinality arising when estimating the two resistances simultaneously. One strategy is to impose an *a priori* constraint on r_a based on our mechanistic understanding (theory-driven strategy), while the other strategy makes use of more observational data and adds a constraint in predicting r_a through multi-task learning of the latent as well as the sensible heat flux (Q_H ; data-driven strategy). Our

31 results show that all hybrid models exhibit a fairly high predictive skill for the target variables with $R^2=$
32 0.82-0.89 for grasslands and $R^2= 0.70$ -0.80 for forests sites at the mean diurnal scale. The predictions
33 of r_s and r_a show physical consistency across the two regularized hybrid models, but are physically
34 implausible in the under-constrained hybrid model. The hybrid models are robust in reproducing
35 consistent results for energy fluxes and resistances across different scales (diurnal, seasonal,
36 interannual), reflecting their ability to learn the physical dependence of the target variables on the
37 meteorological inputs. As a next step, we propose to test these heavily observation-informed
38 parameterizations derived through hybrid modeling as a substitute for overly simple *ad hoc*
39 formulations in Earth system models.

40 Keywords: Hybrid modeling, physics-constrained, machine learning, multi-task learning,
41 evapotranspiration, surface conductance, aerodynamic conductance

42 **1. Introduction**

43 Evapotranspiration, *i.e.* the surface latent heat flux (Q_{LE}), plays a key role in driving Earth's energy,
44 water, and carbon cycles, and is primarily controlled by dynamic meteorological conditions as well as
45 rather static soil properties and plant traits (Jung et al., 2010; Dou & Yang, 2018; Ajami, 2021). The
46 characterization of Q_{LE} , however, remains challenging as our understanding of the underlying processes
47 that control the exchange flux of water between land and atmosphere is still limited (Friedl, 1996;
48 Sellers et al., 1997; Wang & Dickinson, 2012; Chen et al., 2014). While the physical drivers that cause
49 water to evaporate are well described and understood, the influence of the biological control on Q_{LE} ,
50 mainly the transpirative water flux, is more difficult to assess. The key problem is that we cannot
51 formulate universally valid mechanistic laws to describe plant behavior in their interactions between
52 changing atmospheric and soil conditions. As a consequence, empirical formulations, especially for
53 surface and aerodynamic resistance (Polhamus et al., 2013), remain in process-based models, which
54 can lead to large uncertainties in predicting Q_{LE} . In this study, we propose a hybrid modeling approach
55 that allows inference of these biological controls from observational data of Q_{LE} across ecosystems
56 using machine learning, while adhering to known physical laws (Reichstein et al., 2022).

57 Plants critically influence Q_{LE} mainly through their direct control of transpiration, but also through
58 shaping aerodynamic surface properties. Plants use their leaf stomata to dynamically regulate the water

59 loss to the atmosphere, which not only depends on the atmospheric water demand, but also on soil water
60 availability (Damour et al., 2010; Kennedy et al., 2019; Carminati & Javaux, 2020). Simultaneously,
61 plants use the stomata to resorb atmospheric CO₂ as the central ingredient in the photosynthetic process
62 (Schulze, 1986; Chaves et al., 2016). Consequently, most formulations of stomatal conductance (or the
63 inverse, stomatal resistance r_s) are empirical and rely on optimality concepts: minimizing the water loss
64 while maximizing carbon assimilation (e.g. Tan et al., 2021). However, these concepts do not take into
65 account the active transpiration mechanism that some plants use to down-regulate leaf temperature
66 through evaporative cooling to prevent leaf overheating at high irradiance and air temperature (Lin et
67 al., 2017). Other empirical approaches, e.g. the Jarvis–Stewart formulation, aim to derive
68 parametrizations based on statistical correlations between r_s (or canopy resistance) and the key
69 environmental variables (Jarvis, 1976; Stewart, 1988). These *ad hoc* formulations have several
70 drawbacks, e.g., they are considered too rigid, especially when evaluated in a coupled system of
71 atmosphere-biosphere feedbacks where some of the environmental variables are actually also a function
72 of r_s (Ronda et al., 2001).

73 Formulations of how plants affect Q_{LE} by shaping surface roughness and associated aerodynamic
74 properties are considered less uncertain, but vary considerably among vegetation types (Shaw &
75 Pereira, 1982; Nakai et al., 2008; Maurer et al., 2015). Generally, near-surface wind enhances turbulent
76 mixing and thus the exchange of mass and heat between the surface and the atmosphere. The surface
77 roughness lengths — critically determined by plant physiology — influence the mechanical turbulence
78 as well as the near-surface atmospheric thermal structure (Vila-Guerau de Arellano et al., 2015). These
79 relationships are formulated in the aerodynamic resistance r_a , which is conventionally assumed to scale
80 inversely (hyperbola-type function) with wind speed, frictional velocity and atmospheric instability
81 based on the diagnostic empirical Monin–Obukhov similarity theory (Knauer et al., 2018). Several
82 studies (Chehbouni et al., 1996; Liu et al., 2006; Su et al., 2021; Trebs et al., 2021) demonstrated that
83 these parameterizations might work under controlled settings in the laboratory, however, show large
84 discrepancies when applied to other terrain and vegetation types. Overall, such empirical
85 representations for r_s and r_a in deterministic models for Q_{LE} , although generally obeying physical laws
86 and phenomenological behaviour (Krasnopolsky, 2013; de Bezenac et al., 2017), exhibit limited
87 capability to adapt to other or changing vegetation composition and/or long-term climatic conditions,
88 especially with respect to soil moisture (Damour et al., 2010; Medlyn et al., 2011; Kennedy et al., 2019).

89 Statistical models due to their data-adaptive nature have been proposed as alternative approaches
90 to reliably estimate Q_{LE} (Dou & Yang, 2018; Carter & Liang, 2019). In particular, approaches that use
91 machine learning (ML) techniques are gaining traction because they potentially can reveal unknown
92 latent processes or constitute a more complete statistical representation of the processes that influence
93 Q_{LE} at different scales in space and time (Dou & Yang, 2018; Jung et al., 2009, 2020). However, these
94 data-driven models also are subject to several drawbacks, such as the need for large amounts of high-
95 quality data, their usually limited, poor out-of-sample generalizability, and their lack of mechanistic
96 interpretability (Karpatne, Atluri, et al., 2017; Karpatne, Watkins, et al., 2017).

97 By combining machine-learning and mechanistic modeling, here denoted hybrid modeling, allows
98 us to combine the strengths of both techniques: ensure physical consistency while efficiently harvesting
99 the growing resource of observational data (Reichstein et al., 2019, 2022). Several studies have
100 successfully applied hybrid modeling in hydrological applications, such as the characterization of the
101 different known and unknown variables governing the global water cycle (Kraft et al., 2020, 2022),
102 simulation of lake temperature dynamics (Jia et al., 2020), and the modeling of global extreme flooding
103 events (Yang et al., 2019). Other studies focusing on land-atmosphere interactions of ecosystem fluxes,
104 such as Q_{LE} (Zhao et al., 2019), showed that these hybrid approaches allow for better extrapolation
105 capabilities during extreme conditions.

106 In this study we adapt the hybrid modeling approach and develop different models of Q_{LE} using
107 the Penman-Monteith equation (Penman, 1948; Monteith, 1965) and eddy covariance flux
108 measurements from several grassland as well as forest sites (Baldocchi et al., 2001; Li et al., 2018). Our
109 hybrid models not only seek to yield accurate predictions of Q_{LE} , but more importantly enable to learn
110 the functioning and influence of biological processes on Q_{LE} , expressed as the surface (r_s) and
111 aerodynamic resistances (r_a). We present and explore the problem of equifinality in our setting (i.e.
112 many combinations of r_a and r_s can result in the same Q_{LE}) and propose two conceptually different
113 solutions (theory- versus data-driven). We evaluate the predictions of our various hybrid models for
114 Q_{LE} , r_a and r_s against purely statistical models as well as against established mechanistic models. We
115 conclude with the lessons learned.

116 **2. Methodology**

117 2.1 FLUXNET 2015 Data

118 The global flux network (FLUXNET; <https://fluxnet.fluxdata.org>), a global network of eddy
119 covariance (EC) towers, provides estimates of energy, water and carbon fluxes at the land surfaces
120 across climate regimes and plant functional types (Baldocchi et al., 2001; Li et al., 2018). The
121 measurements in the FLUXNET 2015 Tier 1 dataset are resolved at a half-hourly frequency. We select
122 only measured data and omit gap-filled data (Reichstein et al., 2005). Further, we restrict our analysis
123 to energy-balance-corrected measurements, because the EC data do not satisfy the energy balance
124 budget closure which potentially introduces high uncertainty / systematic bias in our results (Wilson et
125 al., 2002). Daytime values are selected based on a threshold of sensible heat flux $Q_H > 5 \text{ Wm}^{-2}$ and
126 incoming short-wave radiation $SW_{in} > 50 \text{ Wm}^{-2}$ to avoid stable boundary layer conditions (Lin et al.,
127 2018; Li et al., 2019). Only positive values are selected for the latent heat flux (Q_{LE}), net radiation (R_n),
128 soil heat flux (Q_G), and vapor pressure deficit (VPD) for daylight data (Zhou et al., 2016), and winter
129 months (between the 10th and 3rd months of the year) are excluded to focus on surface heat fluxes when
130 the vegetation is active (Zhao et al., 2019). The FLUXNET sites chosen include 3 forests and 3
131 grasslands with varying climates, site properties and long-term site year data (Table1).

132 2.2 The physically-based component: Penman-Monteith equation

133 Various process-based models exist for the estimation of Q_{LE} . They can be subdivided into
134 energy, mass transfer-based, water balance methods, and aerodynamic methods (Brutsaert, 2005; Zhao
135 et al., 2013). One prominent example is the Penman-Monteith (PM) equation (Penman, 1948; Monteith,
136 1965) that provides the theoretical basis for determining Q_{LE} , and for showing how Q_{LE} responds to
137 changing climate and vegetation conditions (Monteith & Unsworth, 2013). The estimation of Q_{LE} can
138 be traced back to the model proposed by Penman (1948) which combines the energy balance and mass
139 transfer approaches to estimate evaporation from open water surfaces, which was then extended to
140 vegetative surfaces (Monteith, 1985; Monteith & Unsworth, 2013; Vialet-Chabrand & Lawson, 2019).
141 The PM equation

$$Q_{LE} = \frac{s_c(R_n - Q_G) + \frac{\rho_a c_p (e_s - e_a)}{r_a}}{s_c + \gamma(1 + \frac{r_s}{r_a})}, \quad (1)$$

142 describes the latent heat flux representing Q_{LE} fraction ($\text{MJ m}^{-2} \text{d}^{-1}$). Where R_n is the net radiation
 143 ($\text{MJ m}^{-2} \text{d}^{-1}$), Q_G is the soil heat flux ($\text{MJ m}^{-2} \text{d}^{-1}$), s_c is the slope of the saturation vapor pressure-
 144 temperature relationship (kPa C^{-1}), $e_s - e_a$ is the vapor pressure deficit (VPD) of air (kPa), ρ_a is the
 145 mean air density at constant pressure (kg m^{-3}), c_p is the specific heat of dry air at constant pressure
 146 ($1004.834 \text{ J kg}^{-1} \text{ C}^{-1}$), γ is the psychrometric constant (kPa C^{-1}), r_s is the bulk surface resistance
 147 (sm^{-1}), and r_a is the aerodynamic resistance (sm^{-1}).

148 2.3 Overview of models

149 2.3.1 Inverted Penman-Monteith and Pure ML model

150 The PM equation is considered to be physically-based, since core physiological and aerodynamic
 151 factors describe the evaporative process (Jain et al., 2008). The equation highlights the relationship
 152 between evapotranspiration and surface conductance, which is regulated by the leaf stomata to minimize
 153 the water loss to the atmosphere (Hetherington & Woodward, 2003; Damour et al., 2010; Gerosa et al.,
 154 2012). Extensive approaches exist to model surface conductance at the leaf level. The determination of
 155 surface conductance at the canopy scale, however, is even more challenging due to canopy
 156 heterogeneity and variability in microclimate within the canopy (Bonan et al., 2011). A common
 157 approach thus is to simply to solve the Penman-Monteith equation for r_s to obtain the bulk surface
 158 resistance

$$r_s = \frac{r_a s_c (R_n - Q_G) + \rho_a c_p (e_s - e_a) - r_a Q_{LE} (s_c + \gamma)}{\gamma Q_{LE}}, \quad (2)$$

159 assuming that the aerodynamic resistance r_a is known. The inverted PM equation (PM Inv) is used to
 160 quantify canopy parameters and expresses the relative significance of advective and radiative energy
 161 for Q_{LE} as a function of the ratio of surface to aerodynamic resistance (Kelliher et al., 1992; Köstner et
 162 al., 1992; Zeppel & Eamus, 2008; Zhang et al., 2016). We restrict surface and aerodynamic resistance
 163 values derived using Penman-Monteith inversion and empirical formulations (Knauer et al., 2018)
 164 based on intervals that are physically realistic ($0\text{-}2000 \text{ sm}^{-1}$ and $0\text{-}500 \text{ sm}^{-1}$, respectively).

165 The estimates for r_s from Eq. 2 derived through inverting the PM equation are referred to as the
 166 PM Inv model. Values for r_a are estimated using the Big Leaf package (Knauer et al., 2018), which

167 calculates r_a as the sum of aerodynamic resistance for momentum (r_{am}) and canopy boundary layer
 168 resistance for heat (r_{bh})

$$r_{am} = WS/U^{*2} \quad (3)$$

$$r_{bh} = 6.2 U^{*-0.667} \quad (4)$$

and

$$r_a = r_{am} + r_{bh} , \quad (5)$$

169 where WS is wind speed (ms^{-1}) and U^* is friction velocity (ms^{-1}). The PM Inv model represents a
 170 baseline physical model for comparison against data-driven models for Q_{LE} . The pure ML model for
 171 Q_{LE} is set up to evaluate predictions against hybrid models. The r_s is calculated from Q_{LE} predictions
 172 from the pure ML model by using PM Inv, and r_a is estimated using the *ad hoc* formulation (Eq. 5)
 173 approach. This model is purely data-driven and does not contain any physical constraint regarding Q_{LE} .

174 **2.3.2 Under-constrained hybrid model**

175 The hybrid framework calculates Q_{LE} using the PM equation (ref to equation), where the two
 176 intermediate variables r_s and r_a are estimated by two feed-forward neural networks (FNN)(Fig. 1). The
 177 predictors used for predicting r_s consist of air temperature (TA), water availability index (WAI),
 178 incoming shortwave radiation (SW_{in}), mean incoming shortwave potential ($SW_{pot\ sm}$), vapor pressure
 179 deficit (VPD), net radiation (R_n). The WAI is calculated as the annual cumulative difference between
 180 Q_{LE} and precipitation (P). The WAI at time t (WAI_t) is calculated from the difference between Q_{LE_t}
 181 and P_t and added WAI at previous time step (WAI_{t-1})

$$WAI_t = P_t - Q_{LE_t} + WAI_{t-1} . \quad (6)$$

182 The predictors used for predicting r_a include wind speed (WS) and is friction velocity (U^*). The
 183 predictors are normalized using the mean and standard deviation of the training dataset. Thus, the hybrid
 184 model predicts first the intermediate (also called latent) variables r_s and r_a and uses them to estimate

185 Q_{LE} based on the PM equation. The loss function is hence defined as the difference of mean absolute
 186 Q_{LE} errors between the model predictions and observations with n sample size, and parameters θ for
 187 r_s and r_a

$$\min_{\theta_{r_a}, \theta_{r_s}} \sum_{i=1}^n |\hat{Q}_{LE_i} - Q_{LE_i}|. \quad (7)$$

188 Although the two FNN for r_a and r_s take different predictor variables, the hybrid model is
 189 characterized as under-constrained when simultaneously estimating the two intermediate variables
 190 using only one target Q_{LE} . The proposed hybrid model thus suffers from equifinality in this framework,
 191 so that many different combinations of r_s and r_a can result in the same Q_{LE} value (Fig. 2). The issue of
 192 equifinality, or non-uniqueness, is when different model parametrization and/or structures result in
 193 equivalent representations of the system (Beven, 2006; Schmidt et al., 2020).

194 **2.3.3 Constrained hybrid models: *a priori* and multi-task learning models**

195 The identification and elimination of equifinality due to the non-uniqueness in the physics-based
 196 component is one of the key challenges in hybrid modeling (Kraft et al., 2022). One way to reduce
 197 equifinality is to restrict the parameter space through model regularization (Fig. 3). This may be
 198 achieved by including additional theory, for example by the integration of *a priori* knowledge in the
 199 loss function (i.e. a regularization). Here, we choose to induce an *a priori* constraint on r_a in the hybrid
 200 model based on empirical formulation presented in Eq. 5 as the formulation for r_a are considered to be
 201 more robust than for r_s . To do so we regularize the loss function by adding a constraint on aerodynamic
 202 resistance r_a / ϕ . The relative importance of r_a in the new loss is regulated by ϕ , which is varied between
 203 0.01 (high influence) to 2 (little influence). Based on multiple model runs, with different ϕ values, the
 204 value of $\phi = 2$ was selected for the results presented, thus only imposing a minor influence based on
 205 prior knowledge in the loss function. Another way of restricting the parameter space is by extending
 206 the framework to model auxiliary target variables in a multi-task setting. Since the sensible heat flux
 207 (Q_H) is also dependent on the aerodynamic resistance r_a , we explore multi-task learning approach
 208 (Liebel & Körner, 2018) on the intermediate variable regularization by adding Q_H as an auxiliary target
 209 variable in addition to Q_{LE} (Fig. 3). The estimation of Q_H is based on the resistance formulation

$$Q_H = \frac{\rho_a c_p (TS - TA)}{r_a}, \quad (8)$$

211 where TS and TA are surface and air temperature respectively. The TS is estimated using the Stefan-
 212 Boltzmann equation

$$TS = \sqrt[4]{\frac{Q_{LW_{out}}}{\sigma \epsilon}}, \quad (9)$$

213 Where $Q_{LW_{out}}$ is the outgoing longwave radiation (Wm^{-2}), σ is the Stefan-Boltzmann constant
 214 ($5.789 \times 10^{-8} Wm^{-2}K^{-4}$) and ϵ is emissivity (dimensionless). The emissivity ranges between 0-1, and
 215 the values chosen were based on a sensitivity analyses for each model with the highest predictive
 216 accuracy.

217 **2.4 Evaluation**

218 In total, four models are constructed, three of which are hybrid models, consisting of one under-
 219 constrained and two constrained hybrid models, where the latter consists of either an *a priori* constraint
 220 on r_a or using a multi-task learning approach. For a baseline comparison, we use a pure ML model and
 221 the estimation of the inverted PM equation to evaluate the predictions of the hybrid models. The network
 222 architectures and hyperparameters used are similar for the different models (Table 2 in the
 223 supplementary information). We select the hyperparameters based on manual optimization and tuning.
 224 Evaluation metrics such as the root mean square error (RMSE) and mean absolute error (*MAE*), and
 225 coefficient of determination (R^2) are used to evaluate the model predictions. To highlight the impact of
 226 noise on model performance, we evaluate the model predictions at the half-hourly and 7-day mean
 227 aggregated scale. The intermediate variables are assessed against the key meteorological predictor
 228 variables to scrutinize physical consistency and plausibility. The target variables are assessed against
 229 observations as well as the key meteorological predictor variables to estimate model performance and
 230 interpretability. We conduct five model runs with random initializations for each of the hybrid models
 231 and for one forest site DE-Tha as well as, one grassland site DE-Gri to evaluate model robustness at the
 232 mean diurnal scale. More information can be found in Table 3 of the supplementary information.

233 **3. Results and discussion**

234 **3.1 Statistical performance and mechanistic plausibility of the models**

235 We evaluate predicted Q_{LE} (\hat{Q}_{LE}) from all the hybrid models and the pure ML model against
236 observed Q_{LE} ($Q_{LE_{obs}}$) at half-hourly scale and at 7-day mean aggregates (mean diurnal) for forest (Fig.
237 4) and grassland (Fig. 5) sites. All models reproduce similar Q_{LE} patterns compared to observations
238 with minor differences in performance. For forests (Fig. 4), the more flexible models, the under-
239 constrained hybrid model and pure ML model, exhibit a slightly higher performance ($R^2 = 0.49$) in
240 comparison to the multi-task learning model ($R^2 = 0.48$) and the *a priori* constraint model ($R^2 = 0.46$).
241 For grasslands, the performance of all models is generally higher than for forests. We find that the
242 performance of the multi-task learning model exceeds the performance of the *a priori* constraint model
243 and is similar to the pure ML model ($R^2 = 0.74-0.75$) (Fig. 5). This finding could indicate that our
244 theory-based constraint for r_a might be too rigid and is not supported by observations of the system.
245 Overall, the RMSE ranges from 70-73 Wm^{-2} for forests and 60-71 Wm^{-2} for grasslands at a half-
246 hourly scale for all models. Moreover, the MAE at half-hourly measurements range between 50-53
247 Wm^{-2} for forests and 43-48 Wm^{-2} for grasslands for all models. The multi-task learning model
248 provides predictions for Q_H (\hat{Q}_H) (Fig. 6) of similar accuracy compared to the Q_{LE} predictions for all
249 sites (Fig. 4-5), reaching $R^2 = 0.53$ for forests and $R^2 = 0.68$ for grasslands sites at half-hourly scale.

250 Our results at half-hourly scale are largely impacted by random measurement noise in EC data. To
251 reduce the effect of this instrumental noise source, we aggregate half-hourly predictions in a 7-day
252 window and calculate the mean diurnal cycle. The results presented in this noise-corrected manner
253 demonstrate an even higher fit between $Q_{LE_{obs}}$ versus \hat{Q}_{LE} (Fig. 4-5) and $Q_{H_{obs}}$ versus \hat{Q}_H (Fig. 6) for
254 forests and grasslands. The R^2 coefficient increases across all models by 53-70% for forests and 15-
255 25% for grasslands sites based on the aggregated mean diurnal predictions. Further, the RMSE drops by
256 47-52% for forests, and by 43-48% for grasslands, while MAE also decreases by 47-52% for forests and
257 42-46% for grasslands. Controlling for noise in \hat{Q}_H in the same manner also increases R^2 from 0.68 to
258 0.87 for grasslands, and R^2 from 0.53 to 0.69 for forests (Fig. 6).

259 To assess the physical plausibility of the presented models, we evaluate their predictions of \hat{Q}_{LE}
260 against the key predictor for atmospheric dryness, VPD. In all models, \hat{Q}_{LE} increases sharply at relatively
261 low values of VPD (0-1 kPa), but starts to stabilize and eventually decreases for higher values of VPD
262 (> 1 kPa; Fig 7). This behavior of the models aligns well with other studies that have shown that the
263 transpiration rate increases with increasing VPD at the low and medium range, but starts to decrease
264 again when VPD reaches high values (Buckley, 2005; Massmann et al., 2019; Monteith, 1995; Mott &

265 Peak, 2013). This plant response could reflect their ability to downregulate stomatal conductance as a
266 preemptive measure to decrease water losses and to circumvent damages arising from intense
267 dehydration of the canopy when the lower atmosphere becomes too dry (Farquhar, 1978; Massmann et
268 al., 2019; Vico et al., 2013). Generally, grasslands sites reach higher \hat{Q}_{LE} values than forest sites for the
269 same VPD range. Again, this result could be related to the different plant responses to VPD, since
270 grasses are assumed to exhibit higher surface conductance (lower surface resistance r_s , respectively)
271 compared to forests, resulting in higher transpiration rates (Garratt, 1992; Jarvis & Stewart, 1979). This
272 aspect is discussed further in the next section when evaluating the learned resistances, r_s and r_a .

273 We next evaluate the hybrid models' consistency with respect to interannual variability of Q_{LE} for
274 the different sites. The interannual anomalies are calculated as the difference between the average
275 annual estimates of $Q_{LE_{obs}}$ in the training dataset and the annual estimates of $Q_{LE_{obs}}$ and \hat{Q}_{LE} in the
276 validation and test dataset for the EC data and models, respectively, to evaluate the predictive capacity
277 of the different models (Jung et al., 2009; Besnard et al., 2019). Figures 4 and 5 show the overall fit
278 and performance of the models in predicting interannual anomalies of \hat{Q}_{LE} compared to observed
279 anomalies of $Q_{LE_{obs}}$. The values of R^2 range between 0.47-0.49 for the interannual \hat{Q}_{LE} anomalies for
280 forests and thus exhibit a comparable performance as at the half-hourly frequency (R^2 ranges between
281 0.46-0.49) (Fig. 4). We observe a similar behavior at grassland site: R^2 ranges between 0.65-0.75 at
282 the half-hourly scale and between 0.62-0.74 for the interannual Q_{LE} anomalies (Fig. 5). Overall, the
283 evaluation of the models at multiple temporal scales shows that the models are capable of learning not
284 only the predominant structure of the diurnal and seasonal cycle, but also the subtler year-to-year
285 anomalies. The presented consistency reflects that the models learn the physically correct dependence
286 of the meteorological predictor variables controlling Q_{LE} .

287 **3.2 Evaluation of the learned intermediate variables \hat{r}_s and \hat{r}_a**

288 Next, we evaluate the inference of the Q_{LE} -controlling resistances \hat{r}_s and \hat{r}_a which are treated as
289 intermediate variables in our hybrid approach. First, we plot the inferred estimates of \hat{r}_s and \hat{r}_a against
290 the key meteorological drivers, namely VPD and the frictional velocity U^* , respectively (Fig. 8-9). The
291 behavior of \hat{r}_s against VPD is consistent across all the models and reflects a somewhat similar behavior
292 as presented for \hat{Q}_{LE} . The predicted \hat{r}_s shows a gentle increase at lower ranges of VPD, so the stomata
293 are still open for gas exchange with the atmosphere. However, as VPD increases to higher values, the

294 stomata start to close and thus the surface resistance increases sharply. Further, we find that \hat{r}_s is
295 generally lower for grasslands, which explains the generally higher estimates of Q_{LE} compared to
296 forests, as discussed above (Fig. 7). Another striking finding is that the models seem to be able to
297 identify differences in the physiological functioning across different plant types in controlling \hat{r}_s . For
298 instance, the inferred relationship of \hat{r}_s and VPD is very similar for the two forest sites DE-Tha and
299 FR-LBr, which are dominated by evergreen needle-leaf trees, however, is quite different for the more
300 arid site FR-Pue, which is dominated by evergreen broad-leaf trees (Fig. 8 a-c). There, the hybrid
301 models show that on average r_s rises more steeply with increasing VPD but flattens at very high VPD
302 (compare fit lines in Fig. 8 a-c). Future research will need to determine whether this behavior actually
303 reflects the plants' mechanism for preventing leaf overheating by maintaining some evaporative cooling
304 through the stomata (Lin et al. 2017), or whether it is just an artifact of too sparse data at high VPD.
305 Overall the inferred \hat{r}_s through hybrid modeling (Fig. 8 a-c) is much more precise than its conventional
306 derivation by inverting the Penman-Monteith equation while making assumptions for r_a (Fig. 8d). This
307 aspect constitutes a key advantage of our hybrid approach as opposed to the inversion method, where
308 artificial noise in the flux measurements directly propagates into the inverted estimates of \hat{r}_s resulting
309 in high artificial variability and a bias in \hat{r}_s ranging between 0-30% (Wehr & Saleska, 2021).

310 The inferred relationship for \hat{r}_a against its key driver U^* is not consistent across the hybrid models.
311 The two constrained hybrid models, i.e. multi-task learning (Fig. 8f) and *a priori* constraint (Fig. 8g),
312 consistently reflect the expected negative logarithmic relationship of \hat{r}_a against U^* (Fig. 8-9). In
313 particular, in the case of the hybrid multi-tasking model, this result is promising because the relationship
314 emerges from the observational data alone, without inducing any prespecified knowledge. Furthermore,
315 the two constrained hybrid models show variations of the \hat{r}_a relationship across the sites (Fig. 8f, g and
316 Fig. 9f, g). Thus, they are capable of capturing the canopy heterogeneity across the sites and are more
317 flexible than the conventional rigid parameterizations shown in Fig 8h (forests) and Fig. 9h (grasslands),
318 where r_a is a homogenous function of U^* across the different sites.

319 The under-constrained hybrid model (Fig. 8e), however, illustrates the risk of equifinality and
320 physics-violating results in this approach. In other words, \hat{r}_a exhibits physically inconsistent
321 relationships in the under-constrained model across the sites (Fig. 8e), while the predicted \hat{r}_s and \hat{Q}_{LE}
322 retain physically plausible estimates (Fig. 8a and Fig. 7 g-i, respectively). The issue of equifinality is

323 more prominent in forests than in grasslands, likely because aerodynamic resistance is less dominant in
324 controlling Q_{LE} in forests (Fig 8e and 9e) (Chen & Liu, 2020).

325 The aerodynamic resistance r_a constitutes a critical link in the surface energy balance especially
326 under different environmental and stability conditions, as it has a bearing on both, Q_{LE} and Q_H . There
327 uncertainties in Q_{LE} and Q_H mainly arise from the uncertainty in estimating in r_a for both dense and
328 sparse canopy, and particularly for arid and semi-arid conditions (Trebs et al., 2021). Our multi-task
329 learning hybrid model, however, is able to provide a fairly high accuracy for Q_{LE} and Q_H predictions
330 for grasslands under unstable and semi-arid conditions without overestimating r_a , which has been
331 proven difficult in other modeling efforts (Trebs et al., 2021). For example, the predictions for Q_{LE} (Fig.
332 5) and Q_H (Fig. 6c, d) at the US-Var grassland site, characterized by a dry Mediterranean-type climate
333 (Xu & Baldocchi, 2004; De Kauwe et al., 2017), are fairly accurate and relate to physically consistent
334 r_a predictions.

335 To get an estimate of uncertainty for the inferred relationships for r_s and r_a , we train each model
336 five times with random initializations (ref to methods). The hybrid models show consistent predictions
337 for the relationships for r_s and r_a at mean diurnal scale across the model runs with different
338 initializations. The under-constrained hybrid model is consistent in producing physically
339 uninterpretable r_a for all initializations, especially for forests while the constrained hybrid models are
340 able to reproduce consistently the physically plausible relationships for r_s and r_a . Hence, we show that
341 our hybrid modeling approach yields robust predictions, yet, we stress the caveats related to equifinality
342 in under-constrained model setups.

343 Lastly, we compare the behavior of surface conductance (g_s) against $Q_{LE_{obs}}$ with varying VPD at
344 the mean diurnal scale for the multi-task learning model, the most promising approach, and the
345 conventionally analyzed inverted PM equation for selected sites (Fig. 10). Both agree on a quasi-linear
346 relationship between g_s and $Q_{LE_{obs}}$ with a gradient in g_s (y direction) with changing VPD. So, as VPD
347 increases, the g_s decreases for the same level of evapotranspiration. This is consistent with the findings
348 of Monteith (1995) whereby model estimates reflect the surface feedback response where a decrease in
349 g_s as VPD increases is a result of a direct increase in transpiration lowering leaf water potential (Streck,
350 2003; Mallick et al., 2013, 2016). The general behavior of g_s is similar between the multi-task learning
351 (Fig. 10b, d) model and the PM Inv model (Fig. 10a, c), however, the estimation of g_s alongside

352 changing $Q_{LE_{obs}}$ in the multi-task learning model is less sensitive to noise at low $Q_{LE_{obs}}$ compared to
353 the PM Inv. Overall, g_s based on the inverted PM equation is considerably higher than based on the
354 hybrid modeling approach. The higher estimation could constitute a systematic bias in g_s rooted in the
355 inversion of PM. In particular, for dense canopies, the overestimation could be related to the non-linear
356 relationship of the stomata to light, as is the case for the DE-Tha forest (Fig. 10a) (Campbell, G. S., &
357 Norman, 1998; Irmak, S. et al., 2008). In grasslands, like DE-Gri (Fig. 10c), the overestimation could
358 be attributed to the propagation of measurement error in deriving the energy balance (Wohlfahrt et al.,
359 2009; Knauer et al., 2018). In summary, the multi-task learning model not only provides more confined
360 but also lower estimates for g_s in contrast to widely used inversion method.

361 **4 Conclusions**

362 We present approaches of end-to-end hybrid modeling of latent heat fluxes that can simultaneously
363 retrieve the two controlling intermediate variables — the surface (r_s) and aerodynamic resistance (r_a)
364 — while maintaining physical consistency across different vegetation types. The hybrid models provide
365 reliable predictions compared to measurements of latent heat fluxes at different scales, ranging from
366 daily to seasonal to interannual variations. The cross-scale consistency shows that our model framework
367 is able to learn the physically consistent dependencies between the meteorological input variables and
368 the target fluxes, rather than just the dominant structure of diurnal and seasonal cycles.

369 The main novelty and outcome of our approach are data-driven parameterizations for r_s and r_a jointly
370 estimated by two separate neural networks. We show that the neural networks together can provide
371 many solutions (non-uniqueness) and lead to physically plausible predictions for Q_{LE} fluxes, while
372 presenting physically implausible relationships to the predictors. This non-uniqueness can be mitigated
373 by introducing either more data or theory into the loss function of the hybrid model. Specifically, we
374 make use of two different approaches (*a priori* constraint and multi-task learning) to regularize the
375 parameter space for the neural networks. The resulting relationships for r_s and r_a not only show
376 physically consistent behavior across scales, but also reveal new insights into how the varying
377 resistances control surface energy fluxes.

378 In the determination of r_a , we find considerable variation between sites compared to the very uniform
379 empirical formulations conventionally used. This inter-site spread in the observation-based
380 parameterizations suggests that the conventional empirical formulations are too rigid and do not account
381 for the heterogeneity caused by the specific vegetation canopy structure. Also in the determination of
382 r_s , the parameterizations derived from hybrid modeling show differences between sites, highlighting
383 in particular the different physiological functions of the different plant types. In addition, we detect that

384 these learned parameterizations in the hybrid models exhibit lower stomatal conductance, suggesting
385 that the r_s values usually obtained by inversion of the Penman-Monteith equation may be systematically
386 overestimated.

387 Several approaches have already been proposed to use the growing number of observations to constrain
388 uncertainty in mechanistic model simulations, especially for key unknown plant behavior in the coupled
389 Earth system (Winkler, et al., 2019 a,b). As a next step, we propose to derive parameterizations directly
390 from observations using hybrid modeling, as presented in this study, to replace these *ad hoc*
391 formulations in Earth system models. This approach will not only help reduce uncertainty, but also
392 advance significantly the understanding of biogeochemical processes in land-atmosphere coupling.

393

394 **Code and data availability**

395 All data used in this study are available from public databases or the literature, which can be found
396 with the references provided in the respective “Data and methods” subsection. Processed data and
397 analysis scripts are available from the corresponding author upon request, and the repository will be
398 published together with this article. Correspondence and requests for materials should be addressed to
399 Reda ElGhawi (relghawi@bgc-jena.mpg.de).

400 **Acknowledgements**

401 This research was funded by the European Research Council (ERC) Synergy Grant
402 “Understanding and modeling the Earth System with Machine Learning (USMILE)” under the Horizon
403 2020 research and innovation programme (Grant agreement No. 855187). Gentine acknowledges
404 funding from the National Science Foundation grant, Learning the Earth with Artificial intelligence and
405 Physics (LEAP).

406 **Author contributions**

407 R.E.G., A.J.W. and M.R. designed the study. R.E.G. conducted the analysis. All authors
408 contributed ideas and to the interpretation of the results. R.E.G. and A.J.W. drafted the manuscript with
409 inputs from all authors.

- 411 Ajami, H. (2021). Geohydrology: Global Hydrological Cycle. In *Encyclopedia of Geology* (pp. 393–398).
 412 Elsevier. <https://doi.org/10.1016/b978-0-12-409548-9.12387-5>
- 413 Baldocchi, D., Falge, E., Gu, L., Olson, R., Hollinger, D., Running, S., Anthoni, P., Bernhofer, C., Davis, K.,
 414 Evans, R., Fuentes, J., Goldstein, A., Katul, G., Law, B., Lee, X., Malhi, Y., Meyers, T., Munger, W.,
 415 Oechel, W., ... Wofsy, S. (2001). FLUXNET: A New Tool to Study the Temporal and Spatial Variability
 416 of Ecosystem-Scale Carbon Dioxide, Water Vapor, and Energy Flux Densities. *Bulletin of the American*
 417 *Meteorological Society*, 82(11), 2415–2434. [https://doi.org/10.1175/1520-](https://doi.org/10.1175/1520-0477(2001)082<2415:FANTTS>2.3.CO;2)
 418 [0477\(2001\)082<2415:FANTTS>2.3.CO;2](https://doi.org/10.1175/1520-0477(2001)082<2415:FANTTS>2.3.CO;2)
- 419 Besnard, S., Carvalhais, N., Arain, M. A., Black, A., Brede, B., Buchmann, N., Chen, J., Clevers, J. G. P. W.,
 420 Dutrieux, L. P., Gans, F., Herold, M., Jung, M., Kosugi, Y., Knohl, A., Law, B. E., Paul-Limoges, E.,
 421 Lohila, A., Merbold, L., Rouspard, O., ... Reichstein, M. (2019). Memory effects of climate and
 422 vegetation affecting net ecosystem CO₂ fluxes in global forests. *PLOS ONE*, 14(2), e0211510.
 423 <https://doi.org/10.1371/journal.pone.0211510>
- 424 Beven, K. (2006). A manifesto for the equifinality thesis. *Journal of Hydrology*, 320(1–2), 18–36.
 425 <https://doi.org/10.1016/J.JHYDROL.2005.07.007>
- 426 Bonan, G. B., Lawrence, P. J., Oleson, K. W., Levis, S., Jung, M., Reichstein, M., Lawrence, D. M., &
 427 Swenson, S. C. (2011). Improving canopy processes in the Community Land Model version 4 (CLM4)
 428 using global flux fields empirically inferred from FLUXNET data *Journal of Geophysical Research:*
 429 *Biogeosciences* 116, no. G2 (2011). *Journal of Geophysical Research: Biogeosciences*, 116(G2).
 430 <https://doi.org/10.1029/2010JG001593>
- 431 Brutsaert, W. (2005). *Hydrology: an introduction*. Cambridge University Press.
- 432 Buckley, T. N. (2005). The control of stomata by water balance. *New Phytologist*, 168(2), 275–292.
 433 <https://doi.org/10.1111/J.1469-8137.2005.01543.X>
- 434 Campbell, G. S., & Norman, J. M. (1998). *An Introduction to Environmental Biophysics*. Springer-Verlag.
- 435 Carminati, A., & Javaux, M. (2020). Soil Rather Than Xylem Vulnerability Controls Stomatal Response to
 436 Drought. *Trends in Plant Science*, 25(9), 868–880. <https://doi.org/10.1016/J.TPLANTS.2020.04.003>
- 437 Carter, C., & Liang, S. (2019). Evaluation of ten machine learning methods for estimating terrestrial
 438 evapotranspiration from remote sensing. *International Journal of Applied Earth Observation and*
 439 *Geoinformation*, 78, 86–92. <https://doi.org/10.1016/J.JAG.2019.01.020>
- 440 Chaves, M. M., Costa, J. M., Zarrouk, O., Pinheiro, C., Lopes, C. M., & Pereira, J. S. (2016). Controlling
 441 stomatal aperture in semi-arid regions—The dilemma of saving water or being cool? *Plant Science*, 251,
 442 54–64. <https://doi.org/10.1016/J.PLANTSCI.2016.06.015>
- 443 Chehbouni, A., Lo Seen, D., Njoku, E. G., & Monteny, B. M. (1996). Examination of the difference between
 444 radiative and aerodynamic surface temperatures over sparsely vegetated surfaces. *Remote Sensing of*
 445 *Environment*, 58(2), 177–186. [https://doi.org/10.1016/S0034-4257\(96\)00037-5](https://doi.org/10.1016/S0034-4257(96)00037-5)

- 446 Chen, J. M., & Liu, J. (2020). Evolution of evapotranspiration models using thermal and shortwave remote
447 sensing data. *Remote Sensing of Environment*, 237, 111594. <https://doi.org/10.1016/J.RSE.2019.111594>
- 448 Chen, Y., Xia, J., Liang, S., Feng, J., Fisher, J. B., Li, X., Li, X., Liu, S., Ma, Z., Miyata, A., Mu, Q., Sun, L.,
449 Tang, J., Wang, K., Wen, J., Xue, Y., Yu, G., Zha, T., Zhang, L., ... Yuan, W. (2014). Comparison of
450 satellite-based evapotranspiration models over terrestrial ecosystems in China. *Remote Sensing of*
451 *Environment*, 140, 279–293. <https://doi.org/10.1016/j.rse.2013.08.045>
- 452 Damour, G., Simonneau, T., Cochard, H., & Urban, L. (2010). An overview of models of stomatal conductance
453 at the leaf level. In *Plant, Cell and Environment* (Vol. 33, Issue 9, pp. 1419–1438). Plant Cell Environ.
454 <https://doi.org/10.1111/j.1365-3040.2010.02181.x>
- 455 de Bezenac, E., Pajot, A., & Gallinari, P. (2017). Deep Learning for Physical Processes: Incorporating Prior
456 Scientific Knowledge. *ArXiv*. <http://arxiv.org/abs/1711.07970>
- 457 De Kauwe, M. G., Medlyn, B. E., Knauer, J., & Williams, C. A. (2017). Ideas and perspectives: How coupled is
458 the vegetation to the boundary layer? *Biogeosciences*, 14(19), 4435–4453. [https://doi.org/10.5194/BG-14-](https://doi.org/10.5194/BG-14-4435-2017)
459 4435-2017
- 460 Dou, X., & Yang, Y. (2018). Evapotranspiration estimation using four different machine learning approaches in
461 different terrestrial ecosystems. *Computers and Electronics in Agriculture*, 148, 95–106.
462 <https://doi.org/10.1016/j.compag.2018.03.010>
- 463 Farquhar, G. D. (1978). Feedforward Responses of Stomata to Humidity. *Functional Plant Biology*, 5(6), 787–
464 800. <https://doi.org/10.1071/PP9780787>
- 465 Friedl, M. A. (1996). Relationships among remotely sensed data, surface energy balance, and area-averaged
466 fluxes over partially vegetated land surfaces. *Journal of Applied Meteorology and Climatology*, 35(11),
467 2091–2103. [https://doi.org/10.1175/1520-0450\(1996\)035<2091:RARSDDS>2.0.CO;2](https://doi.org/10.1175/1520-0450(1996)035<2091:RARSDDS>2.0.CO;2)
- 468 Garratt, J. R. (1992). *The Atmospheric Boundary Layer*. Cambridge University Press.
- 469 Gerosa, G., Mereu, S., Finco, A., & Marzuoli, R. (2012). Stomatal Conductance Modeling to Estimate the
470 Evapotranspiration of Natural and Agricultural Ecosystems. In *Evapotranspiration - Remote Sensing and*
471 *Modeling*. InTech. <https://doi.org/10.5772/21825>
- 472 Halladay, K., & Good, P. (2017). Non-linear interactions between CO₂ radiative and physiological effects on
473 Amazonian evapotranspiration in an Earth system model. *Climate Dynamics*, 49(7–8), 2471–2490.
474 <https://doi.org/10.1007/s00382-016-3449-0>
- 475 Hetherington, A. M., & Woodward, F. I. (2003). The role of stomata in sensing and driving environmental
476 change. *Nature*, 424(6951), 901–908. <https://doi.org/10.1038/nature01843>
- 477 Irmak, S., M., Irmak, A., Arkebauer, T. J., Weiss, A., Martin, D. L., & Eisenhauer, D. E. (2008). On the scaling
478 up leaf stomatal resistance to canopy resistance using photosynthetic photon flux density. *Agricultural and*
479 *Forest Meteorology*, 148(6–7), 1034–1044.
- 480 Jain, S. K., Nayak, P. C., & Sudheer, K. P. (2008). Models for estimating evapotranspiration using artificial

- 481 neural networks, and their physical interpretation. *Hydrological Processes*, 22(13), 2225–2234.
482 <https://doi.org/10.1002/hyp.6819>
- 483 Jarvis, P. G. (1976). The interpretation of the variations in leaf water potential and stomatal conductance found
484 in canopies in the field. *Philosophical Transactions of the Royal Society of London. B, Biological*
485 *Sciences*, 273(927), 593–610. <https://doi.org/10.1098/RSTB.1976.0035>
- 486 Jarvis, P. G., & Stewart, J. B. (1979). Evaporation of water from plantation forest. *D. Ford, D.C. Malcolm, J.*
487 *Atterson (Eds.), The Ecology of Even-Aged Forest Plantations, Institute of Terrestrial Ecology,*
488 *Cambridge*, 327–350.
- 489 Jia, X., Zwart, J., Sadler, J., Appling, A., Oliver, S., Markstrom, S., Willard, J., Xu, S., Steinbach, M., Read, J.,
490 & Kumar, V. (2020). Physics-Guided Recurrent Graph Model for Predicting Flow and Temperature in
491 River Networks. *ArXiv Preprint*.
- 492 Jung, M., Reichstein, M., & Bondeau, A. (2009). Towards global empirical upscaling of FLUXNET eddy
493 covariance observations: Validation of a model tree ensemble approach using a biosphere model.
494 *Biogeosciences*, 6(10), 2001–2013. <https://doi.org/10.5194/BG-6-2001-2009>
- 495 Jung, M., Reichstein, M., Ciais, P., Seneviratne, S. I., Sheffield, J., Goulden, M. L., Bonan, G., Cescatti, A.,
496 Chen, J., De Jeu, R., Dolman, A. J., Eugster, W., Gerten, D., Gianelle, D., Gobron, N., Heinke, J.,
497 Kimball, J., Law, B. E., Montagnani, L., ... Zhang, K. (2010). Recent decline in the global land
498 evapotranspiration trend due to limited moisture supply. *Nature*, 467(7318), 951–954.
499 <https://doi.org/10.1038/nature09396>
- 500 Jung, M., Schwalm, C., Migliavacca, M., Walther, S., Camps-Valls, G., Koirala, S., Anthoni, P., Besnard, S.,
501 Bodesheim, P., Carvalhais, N., Chevallier, F., Gans, F., S Goll, D., Haverd, V., Köhler, P., Ichii, K., K
502 Jain, A., Liu, J., Lombardozzi, D., ... Reichstein, M. (2020). Scaling carbon fluxes from eddy covariance
503 sites to globe: Synthesis and evaluation of the FLUXCOM approach. *Biogeosciences*, 17(5), 1343–1365.
504 <https://doi.org/10.5194/bg-17-1343-2020>
- 505 Karpatne, A., Atluri, G., Faghmous, J. H., Steinbach, M., Banerjee, A., Ganguly, A., Shekhar, S., Samatova, N.,
506 & Kumar, V. (2017). Theory-guided data science: A new paradigm for scientific discovery from data.
507 *IEEE Transactions on Knowledge and Data Engineering*, 29(10), 2318–2.
- 508 Karpatne, A., Watkins, W., Read, J., & Kumar, V. (2017). Physics-guided Neural Networks (PGNN): An
509 Application in Lake Temperature Modeling. *ArXiv*. <http://arxiv.org/abs/1710.11431>
- 510 Kelliher, F. M., Köstner, B. M. M., Hollinger, D. Y., Byers, J. N., Hunt, J. E., McSeveny, T. M., Meserth, R.,
511 Weir, P. L., & Schulze, E. D. (1992). Evaporation, xylem sap flow, and tree transpiration in a New
512 Zealand broad-leaved forest. *Agricultural and Forest Meteorology*, 62(1–2), 53–73.
513 [https://doi.org/10.1016/0168-1923\(92\)90005-O](https://doi.org/10.1016/0168-1923(92)90005-O)
- 514 Kennedy, D., Swenson, S., Oleson, K. W., Lawrence, D. M., Fisher, R., Lola da Costa, A. C., & Gentine, P.
515 (2019). Implementing Plant Hydraulics in the Community Land Model, Version 5. *Journal of Advances in*
516 *Modeling Earth Systems*, 11(2), 485–513. <https://doi.org/10.1029/2018MS001500>
- 517 Knauer, J., El-Madany, T. S., Zaehle, S., & Migliavacca, M. (2018). Bigleaf—An R package for the calculation
518 of physical and physiological ecosystem properties from eddy covariance data. *PLOS ONE*, 13(8),

- 556 biophysical controls of transpiration and evaporation in the Amazon Basin. *Hydrology and Earth System*
557 *Sciences*, 20(10), 4237–4264. <https://doi.org/10.5194/HESS-20-4237-2016>
- 558 Massmann, A., Gentine, P., & Lin, C. (2019). When Does Vapor Pressure Deficit Drive or Reduce
559 Evapotranspiration? *Journal of Advances in Modeling Earth Systems*, 11(10), 3305–3320.
560 <https://doi.org/10.1029/2019MS001790>
- 561 Maurer, K. D., Bohrer, G., Kenny, W. T., & Ivanov, V. Y. (2015). Large-eddy simulations of surface roughness
562 parameter sensitivity to canopy-structure characteristics. *Biogeosciences*, 12(8), 2533–2548.
563 <https://doi.org/10.5194/BG-12-2533-2015>
- 564 Medlyn, B. E., Duursma, R. A., Eamus, D., Ellsworth, D. S., Prentice, I. C., Barton, C. V. M., Crous, K. Y., De
565 Angelis, P., Freeman, M., & Wingate, L. (2011). Reconciling the optimal and empirical approaches to
566 modelling stomatal conductance. *Global Change Biology*, 17(6), 2134–2144.
567 <https://doi.org/10.1111/J.1365-2486.2010.02375.X>
- 568 Monteith, J. L. (1995). A reinterpretation of stomatal responses to humidity. *Plant, Cell & Environment*, 18(4),
569 357–364. <https://doi.org/10.1111/J.1365-3040.1995.TB00371.X>
- 570 Monteith, J. L. (1965). Evaporation and environment. *Fogg (Ed.), Symposium of the Society for Experimental*
571 *Biology, The State and Movement of Water in Living Organisms, Vol. 19*, 205–234.
- 572 Monteith, J. L. (1985). Evaporation from land surfaces: progress in analysis and prediction since 1948. In:
573 *Advances in Evapotranspiration, Proc. National Conference on Advances in Evapotranspiration. Am.:*
574 *Soc. Agric. Eng., St. Joseph, MI, Chicago, IL*, 4–12. [https://agris.fao.org/agris-](https://agris.fao.org/agris-search/search.do?recordID=US8644525)
575 [search/search.do?recordID=US8644525](https://agris.fao.org/agris-search/search.do?recordID=US8644525)
- 576 Monteith, J. L., & Unsworth, M. (2013). *Principles of environmental physics: plants, animals, and the*
577 *atmosphere* (Fourth). Elsevier Ltd.
- 578 Mott, K. A., & Peak, D. (2013). Testing a vapour-phase model of stomatal responses to humidity. *Plant, Cell &*
579 *Environment*, 36(5), 936–944. <https://doi.org/10.1111/PCE.12026>
- 580 Mystakidis, S., Davin, E. L., Gruber, N., & Seneviratne, S. I. (2016). Constraining future terrestrial carbon cycle
581 projections using observation-based water and carbon flux estimates. *Global Change Biology*, 22(6),
582 2198–2215. <https://doi.org/10.1111/gcb.13217>
- 583 Nakai, T., Sumida, A., Daikoku, K., Matsumoto, K., van der Molen, M. K., Kodama, Y., Kononov, A. V.,
584 Maximov, T. C., Dolman, A. J., Yabuki, H., Hara, T., & Ohta, T. (2008). Parameterisation of aerodynamic
585 roughness over boreal, cool- and warm-temperate forests. *Agricultural and Forest Meteorology*, 148(12),
586 1916–1925. <https://doi.org/10.1016/J.AGRFORMET.2008.03.009>
- 587 Penman, H. L. (1948). Natural evaporation from open water, bare soil and grass. *Proceedings of the Royal*
588 *Society of London. Series A, Mathematical and Physical Sciences*, 193(1032), 120–145.
589 <https://doi.org/10.1098/rspa.1948.0037>
- 590 Polhamus, A., Fisher, J. B., & Tu, K. P. (2013). What controls the error structure in evapotranspiration models?
591 *Agricultural and Forest Meteorology*, 169, 12–24. <https://doi.org/10.1016/j.agrformet.2012.10.002>

- 592 Reichstein, M., Ahrens, B., Kraft, B., Camps-Valls, G., Carvalhais, N., Gans, F., Gentine, P., & Winkler, A. J.
593 (2022). Combining System Modeling and Machine Learning into Hybrid Ecosystem Modeling.
594 *Knowledge-Guided Machine Learning*, 327–352. <https://doi.org/10.1201/9781003143376-14>
- 595 Reichstein, M., Camps-Valls, G., Stevens, B., Jung, M., Denzler, J., Carvalhais, N., & Prabhat. (2019). Deep
596 learning and process understanding for data-driven Earth system science. *Nature*, 566(7743), 195–204.
597 <https://doi.org/10.1038/s41586-019-0912-1>
- 598 Reichstein, M., Falge, E., Baldocchi, D., Papale, D., Aubinet, M., Berbigier, P., Bernhofer, C., Buchmann, N.,
599 Gilmanov, T., Granier, A., Grunwald, T., Havrankova, K., Ilvesniemi, H., Janous, D., Knohl, A., Laurila,
600 T., Lohila, A., Loustau, D., Matteucci, G., ... Valentini, R. (2005). On the separation of net ecosystem
601 exchange into assimilation and ecosystem respiration: review and improved algorithm. *Global Change*
602 *Biology*, 11(9), 1424–1439. <https://doi.org/10.1111/j.1365-2486.2005.001002.x>
- 603 Ronda, R. J., De Bruin, H. A. R., & Holtslag, A. A. M. (2001). Representation of the canopy conductance in
604 modeling the surface energy budget for low vegetation. *Journal of Applied Meteorology*, 40(8), 1431–
605 1444.
- 606 Schmidt, L., Heße, F., Attinger, S., & Kumar, R. (2020). Challenges in Applying Machine Learning Models for
607 Hydrological Inference: A Case Study for Flooding Events Across Germany. *Water Resources Research*,
608 56(5), e2019WR025924. <https://doi.org/10.1029/2019WR025924>
- 609 Schulze, E. D. (1986). Carbon dioxide and water vapor exchange in response to drought in the atmosphere and
610 in the soil. *Annu. Rev. Plant Physiol.; (United States)*, 37(1), 247–274.
611 <https://doi.org/10.1146/ANNUREV.PP.37.060186.001335>
- 612 Sellers, P. J., Dickinson, R. E., Randall, D. A., Betts, A. K., Hall, F. G., Berry, J. A., Collatz, G. J., Denning, A.
613 S., Mooney, H. A., Nobre, C. A., Sato, N., Field, C. B., & Henderson-Sellers, A. (1997). Modeling the
614 exchanges of energy, water, and carbon between continents and the atmosphere. In *Science* (Vol. 275,
615 Issue 5299, pp. 502–509). American Association for the Advancement of Science.
616 <https://doi.org/10.1126/science.275.5299.502>
- 617 Shaw, R. H., & Pereira, A. R. (1982). Aerodynamic roughness of a plant canopy: A numerical experiment.
618 *Agricultural Meteorology*, 26(1), 51–65. [https://doi.org/10.1016/0002-1571\(82\)90057-7](https://doi.org/10.1016/0002-1571(82)90057-7)
- 619 Stewart, J. B. (1988). Modelling surface conductance of pine forest. *Agricultural and Forest Meteorology*,
620 43(1), 19–35. [https://doi.org/10.1016/0168-1923\(88\)90003-2](https://doi.org/10.1016/0168-1923(88)90003-2)
- 621 Streck, N. A. (2003). Stomatal response to water vapor pressure deficit: an unsolved issue. *Current Agricultural*
622 *Science and Technology*, 9(4), 317–322.
- 623 Su, Y., Zhang, C., Chen, X., Liu, L., Ciais, P., Peng, J., Wu, S., Wu, J., Shang, J., Wang, Y., Yuan, W., Yang,
624 Y., Wu, Z., & Laforteza, R. (2021). Aerodynamic resistance and Bowen ratio explain the biophysical
625 effects of forest cover on understory air and soil temperatures at the global scale. *Agricultural and Forest*
626 *Meteorology*, 308–309, 108615. <https://doi.org/10.1016/J.AGRFORMET.2021.108615>
- 627 Tan, S., Wang, H., Prentice, I. C., & Yang, K. (2021). Land-surface evapotranspiration derived from a first-
628 principles primary production model. *Environmental Research Letters*, 16(10), 104047.
629 <https://doi.org/10.1088/1748-9326/AC29EB>

- 630 Trebs, I., Mallick, K., Bhattarai, N., Sulis, M., Cleverly, J., Woodgate, W., Silberstein, R., Hinko-Najera, N.,
631 Beringer, J., Meyer, W. S., Su, Z., & Boulet, G. (2021). The role of aerodynamic resistance in thermal
632 remote sensing-based evapotranspiration models. *Remote Sensing of Environment*, 264, 112602.
633 <https://doi.org/10.1016/J.RSE.2021.112602>
- 634 Vialet-Chabrand, S., & Lawson, T. (2019). Dynamic leaf energy balance: deriving stomatal conductance from
635 thermal imaging in a dynamic environment. *Journal of Experimental Botany*, 70(10), 2839.
636 <https://doi.org/10.1093/JXB/ERZ068>
- 637 Vico, G., Manzoni, S., Palmroth, S., Weih, M., & Katul, G. (2013). A perspective on optimal leaf stomatal
638 conductance under CO₂ and light co-limitations. *Agricultural and Forest Meteorology*, 182–183, 191–
639 199. <https://doi.org/10.1016/J.AGRFORMET.2013.07.005>
- 640 Vila-Guerau de Arellano, J., C. van Heerwaarden, C., J. H. van Stratum, B., & van den Dries, K. (2015).
641 *Atmospheric Boundary Layer*. Cambridge University Press. <https://doi.org/10.1017/CBO9781316117422>
- 642 Wang, K., & Dickinson, R. E. (2012). A review of global terrestrial evapotranspiration: Observation, modeling,
643 climatology, and climatic variability. *Reviews of Geophysics*, 50(2).
644 <https://doi.org/10.1029/2011RG000373>
- 645 Wehr, R., & Saleska, S. R. (2021). Calculating canopy stomatal conductance from eddy covariance
646 measurements, in light of the energy budget closure problem. *Biogeosciences*, 18(1), 13–24.
647 <https://doi.org/10.5194/BG-18-13-2021>
- 648 Winkler, A. J., Myneni, R. B., Alexandrov, G. A., & Brovkin, V. (2019). Earth system models underestimate
649 carbon fixation by plants in the high latitudes. *Nature Communications* 2019 10:1, 10(1), 1–8.
650 <https://doi.org/10.1038/s41467-019-08633-z>
- 651 Winkler, A. J., Myneni, R. B., & Brovkin, V. (2019). Investigating the applicability of emergent constraints.
652 *Earth System Dynamics*, 10(3), 501–523. <https://doi.org/10.5194/ESD-10-501-2019>
- 653 Wohlfahrt, G., Haslwanter, A., Hörtnagl, L., Jasoni, R. L., Fenstermaker, L. F., Arnone, J. A., & Hammerle, A.
654 (2009). On the consequences of the energy imbalance for calculating surface conductance to water vapour.
655 *Agricultural and Forest Meteorology*, 149(9), 1556–1559.
656 <https://doi.org/10.1016/J.AGRFORMET.2009.03.015>
- 657 Xu, L., & Baldocchi, D. D. (2004). Seasonal variation in carbon dioxide exchange over a Mediterranean annual
658 grassland in California. *Agricultural and Forest Meteorology*, 123(1–2), 79–96.
659 <https://doi.org/10.1016/J.AGRFORMET.2003.10.004>
- 660 Yang, T., Sun, F., Gentine, P., Liu, W., Wang, H., Yin, J., Du, M., & Liu, C. (2019). Evaluation and machine
661 learning improvement of global hydrological model-based flood simulations. *Environmental Research*
662 *Letters*, 14(11), 114027. <https://doi.org/10.1088/1748-9326/ab4d5e>
- 663 Zeppel, M., & Eamus, D. (2008). Coordination of leaf area, sapwood area and canopy conductance leads to
664 species convergence of tree water use in a remnant evergreen woodland. *Australian Journal of Botany*,
665 56(2), 97–108. <https://doi.org/10.1071/BT07091>
- 666 Zhang, Z. Z., Zhao, P., McCarthy, H. R., Zhao, X. H., Niu, J. F., Zhu, L. W., Ni, G. Y., Ouyang, L., & Huang,

667 Y. Q. (2016). Influence of the decoupling degree on the estimation of canopy stomatal conductance for
668 two broadleaf tree species. *Agricultural and Forest Meteorology*, 221, 230–241.
669 <https://doi.org/10.1016/J.AGRFORMET.2016.02.018>

670 Zhao, L., Xia, J., Xu, C. yu, Wang, Z., Sobkowiak, L., & Long, C. (2013). Evapotranspiration estimation
671 methods in hydrological models. *Journal of Geographical Sciences* 2013 23:2, 23(2), 359–369.
672 <https://doi.org/10.1007/S11442-013-1015-9>

673 Zhao, W. L., Gentine, P., Reichstein, M., Zhang, Y., Zhou, S., Wen, Y., Lin, C., Li, X., & Qiu, G. Y. (2019).
674 Physics-Constrained Machine Learning of Evapotranspiration. *Geophysical Research Letters*, 46(24),
675 14496–14507. <https://doi.org/10.1029/2019GL085291>

676 Zhou, S., Yu, B., Zhang, Y., Huang, Y., & Wang, G. (2016). Partitioning evapotranspiration based on the
677 concept of underlying water use efficiency. *Water Resources Research*, 52(2), 1160–1175.
678 <https://doi.org/10.1002/2015WR017766>

679

680

681

682

683

684

685

686

687

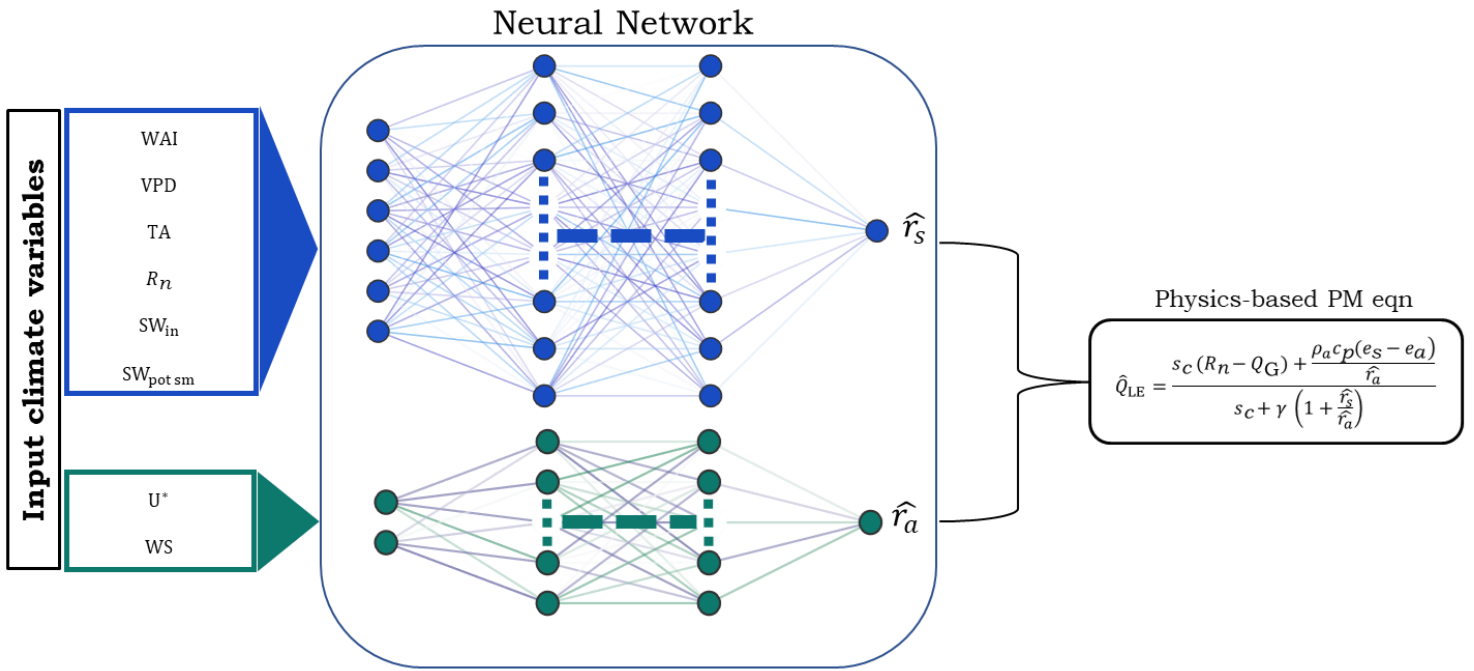
688

689

691 Table 1: Detailed description of each site used derived from the FLUXNET 2015 Tier 1 data.

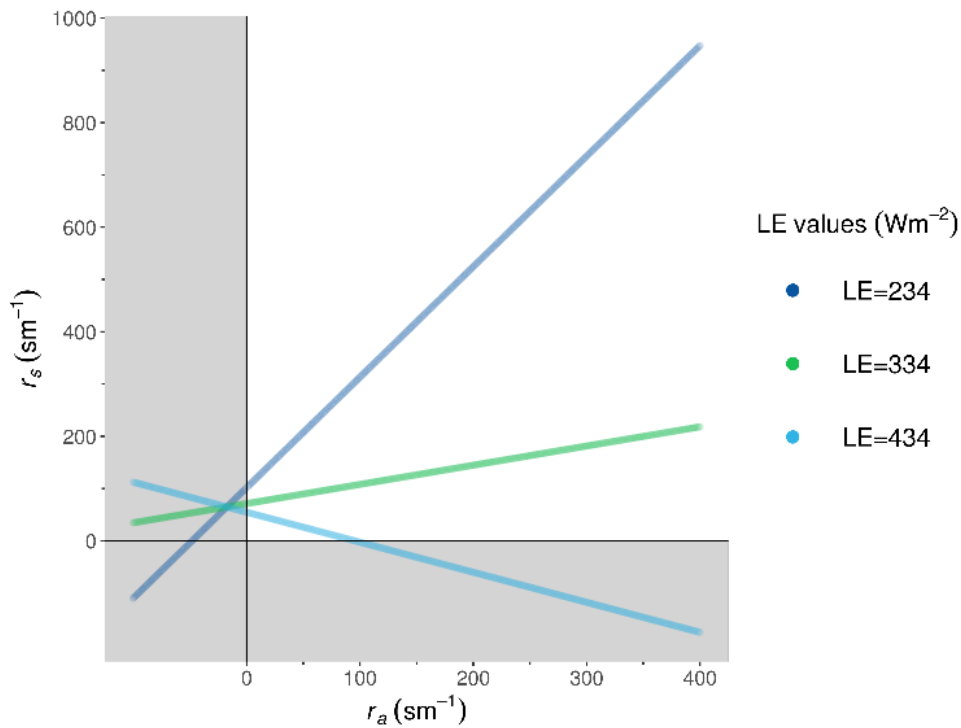
Site ID	IGBP	Elevation (m)	Mean Annual Temperature (°C)	Mean Annual Precipitation (mm)	Data Availability	DOI
DE-Tha	ENF ¹	385	8.2	843	19 years (1996 - 2014)	Christian Bernhofer, Thomas Grünwald, Uta Moderow, Markus Hehn, Uwe Eichelmann, Heiko Prasse, Udo Postel (1996-2014) FLUXNET2015 DE-Tha Tharandt, Dataset. https://doi.org/10.18140/FLX/1440152
FR-Pue	EBF ²	270	13.5	883	15 years (2000 - 2014)	Jean-Marc Ourcival, Karim Piquemal, Richard Joffre, Limousin Jean-Marc (2000-2014) FLUXNET2015 FR-Pue Puechabon, Dataset. https://doi.org/10.18140/FLX/1440164
FR-LBr	ENF ¹	61	13.6	900	12 years (1996 - 2008)	Paul Berbigier, Jean Bonnefond, Alexandre Bosc, Pierre Trichet, Denis Loustau (1996-2008) FLUXNET2015 FR-LBr Le Bray, Dataset. https://doi.org/10.18140/FLX/1440163
CH-Cha	GRA ³	393	9.5	1136	10 years (2005 - 2014)	Lutz Merbold, Kathrin Fuchs, Nina Buchmann, Lukas Hörtnagl (2012-2016) FLUXNET-CH4 CH-Cha Chamau, Dataset. https://doi.org/10.18140/FLX/1669629
DE-Gri	GRA ³	385	7.8	901	11 years (2004 - 2014)	Christian Bernhofer, Thomas Grünwald, Uta Moderow, Markus Hehn, Uwe Eichelmann, Heiko Prasse, Udo Postel () FLUXNET2015 DE-Gri , Dataset. https://doi.org/10.18140/FLX/1440147
US-Var	GRA ³	129	15.8	559	15 years (2000 - 2014)	(2000-2014) FLUXNET2015 US-Var Vaira Ranch- Ione, Dataset. https://doi.org/10.18140/FLX/1440094

- 692 1. ENF (Evergreen Needleleaf Forests: Lands dominated by woody vegetation with a percent cover >60% and height
693 exceeding 2 meters. Almost all trees remain green all year. Canopy is never without green foliage).
694 2. EBF (Evergreen Broadleaf Forests: Lands dominated by woody vegetation with a percent cover >60% and height
695 exceeding 2 meters. Almost all trees and shrubs remain green year-round. Canopy is never without green foliage).
696 3. GRA (Grasslands: Lands with herbaceous types of cover. Tree and shrub cover is less than 10%. Permanent
697 wetlands lands with a permanent mixture of water and herbaceous or woody vegetation. The vegetation can be
698 present in either salt, brackish, or fresh water.)

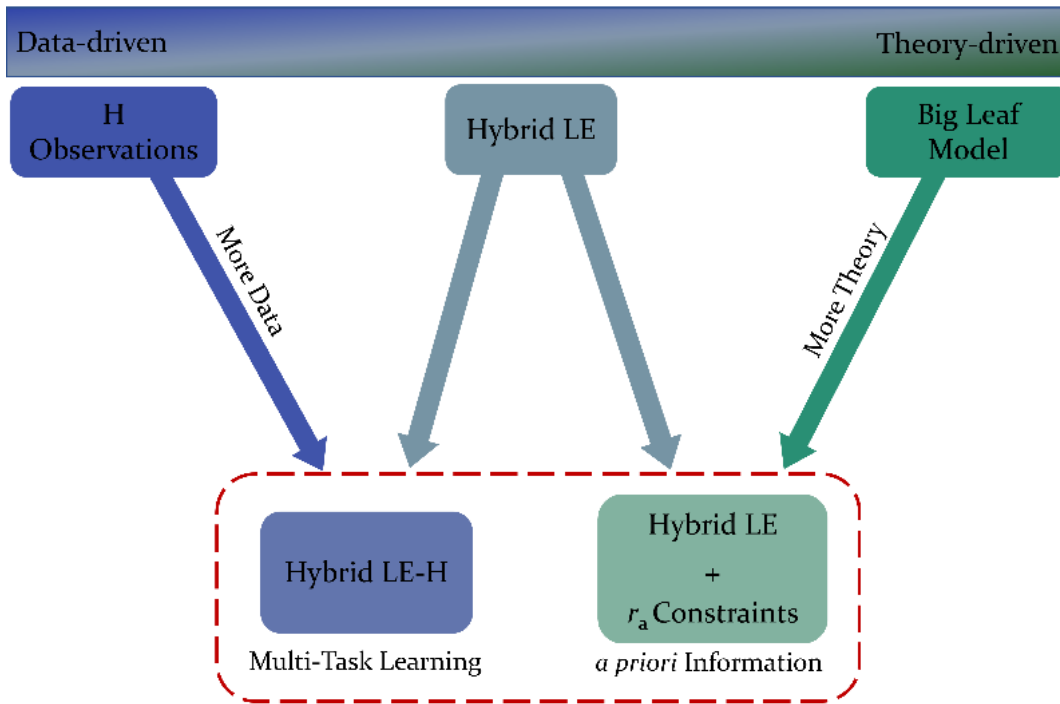


700
 Figure 1: Architecture of the basic hybrid model consists of two neural networks, which estimate r_s and r_a individually with independent input climate variables. The latent variables are used in the Penman-Monteith equation to estimate the latent heat flux (Q_{LE}), and the objective function minimizes losses for Q_{LE} .

701
 702
 703



717
 Figure 2: Equifinality in the physics-based component of hybrid model: The lines represent different Q_{LE} values that can exist for specific conditions (the actual Q_{LE} value is approximately $334 Wm^{-2}$). Fixing all parameters of the PM equation $s_c = 0.175 kPaC^{-1}$, $R_n = 520.38 Wm^{-2}$, $Q_G = 18.51 Wm^{-2}$, $VPD = 1.333 kPa$, $\rho_a = 1.143 kg m^{-3}$, $c_p = 1004.834 J kg^{-1} C^{-1}$, $\gamma = 0.0644 kPaC^{-1}$, the different combinations of r_s and r_a values lead to the same Q_{LE} . Shaded areas show the physically non-plausible and non-realistic values for r_s and r_a combinations, and non-shaded areas show physically plausible values.



730
 Figure 3: Proposed methods for constraining the hybrid model: Right-side shows the theory-driven hybrid model with *a priori* constraint for r_a from the Big Leaf model. Left-side shows data-driven hybrid model with more information from learning an additional target variable Q_H through multi-task learning.

731

732

733

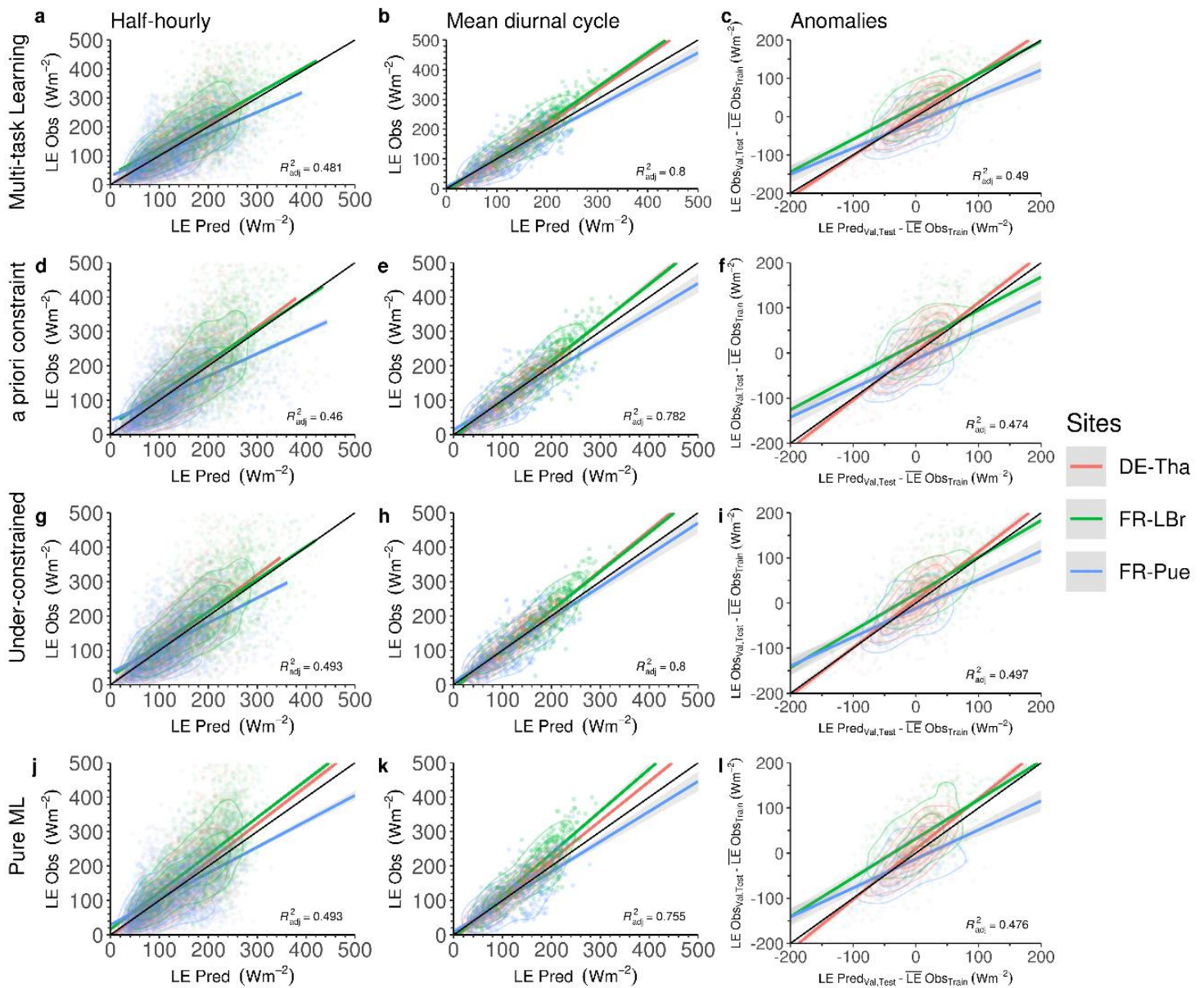
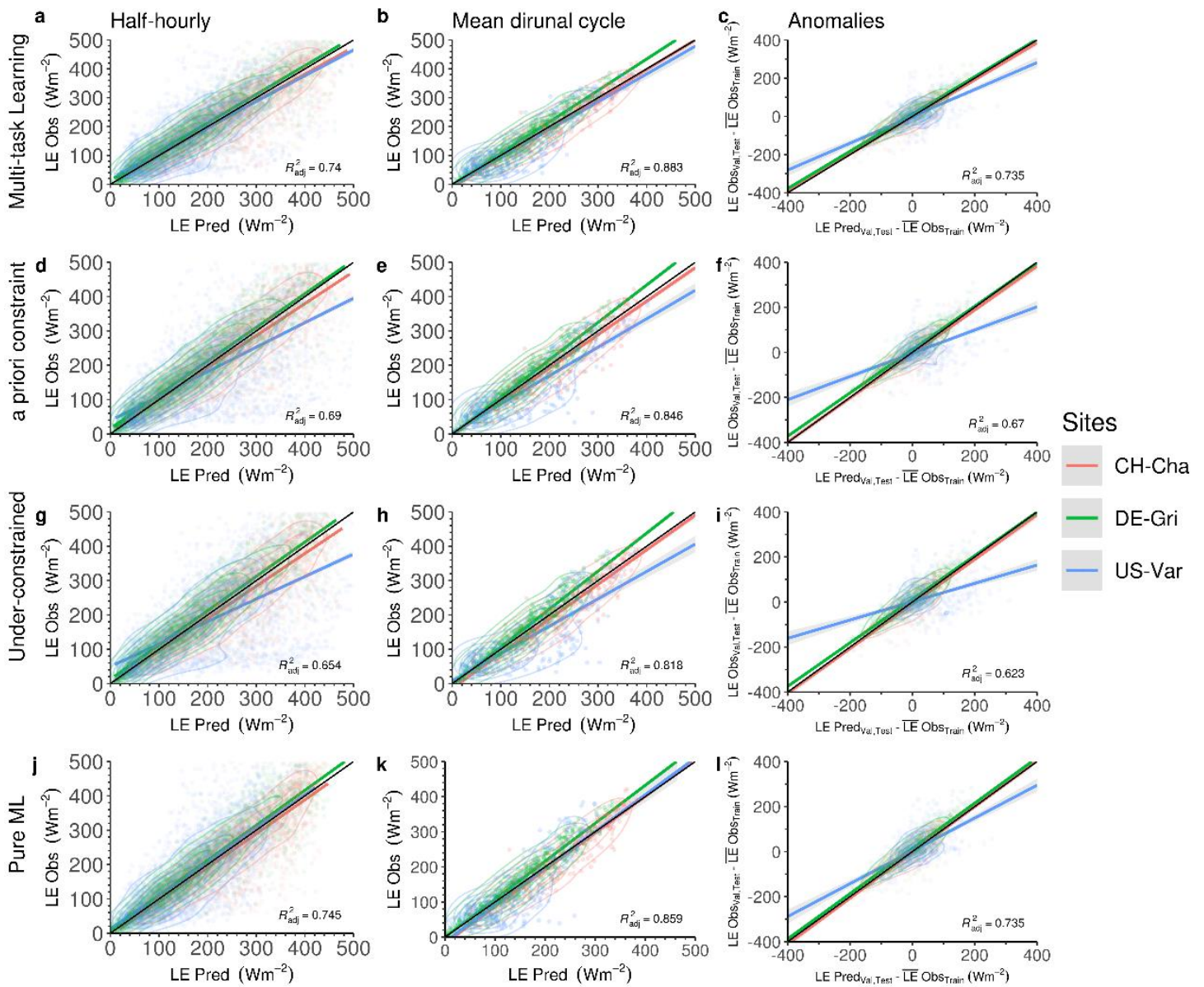
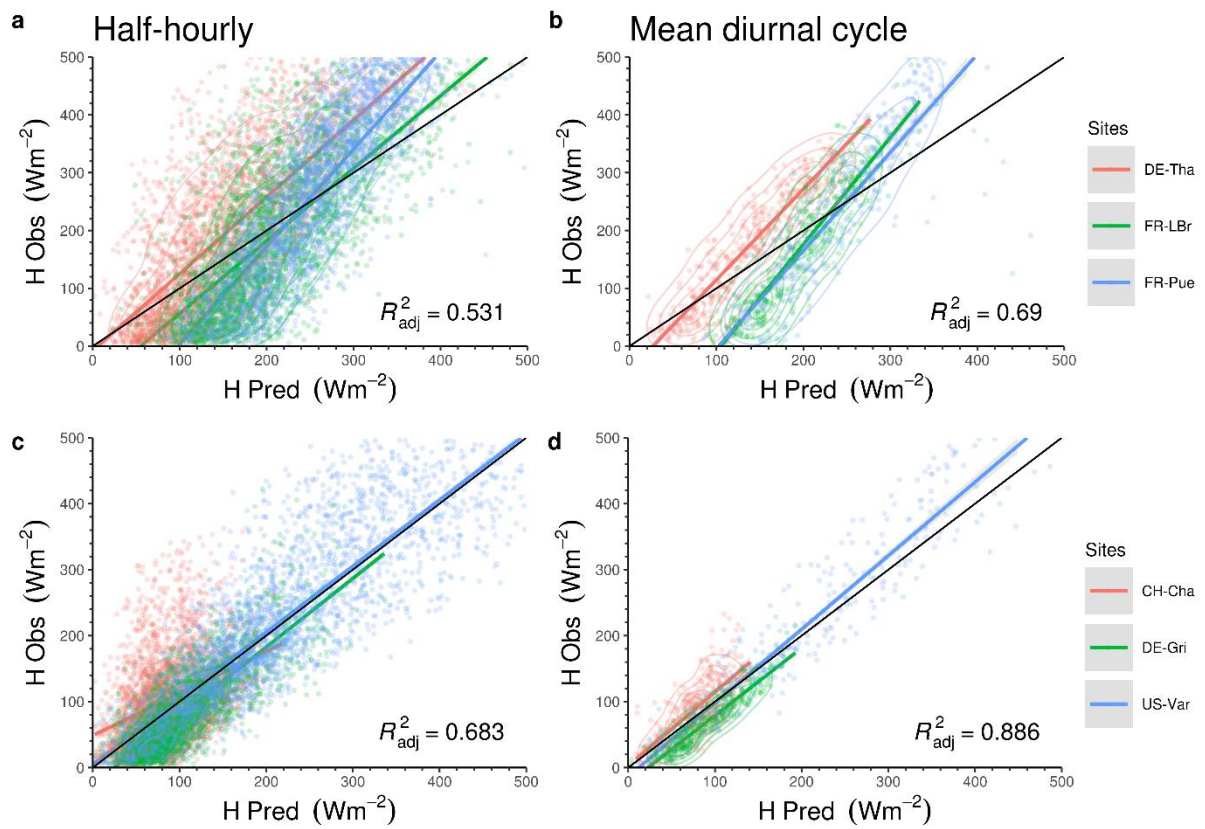


Figure 4: Evaluation of Q_{LE} observations and predictions at different temporal scales for forests. a,d,g,j show predictions against observations at a half-hourly scale for different models; b,e,h,k show predictions against observations at mean diurnal scale; c,f,i,l show Q_{LE} anomalies at interannual scale for the different models.



738 Figure 5: Evaluation of Q_{LE} observations and predictions at different temporal scales for grasslands. a,d,g,j show predictions against observations at a half-hourly scale for different models. b,e,h,k show predictions against observations at mean diurnal scale. c,f,i,l show Q_{LE} anomalies at interannual scale for the different models.



739

Figure 6: Evaluation of Q_H observations and predictions at half-hourly, and mean diurnal scale for forest (a,b) and grasslands (c,d) for multi-task learning hybrid model. Q_H predictions are similar in range compare to Q_{LE} predictions in figures 4-5 for forests and grasslands.

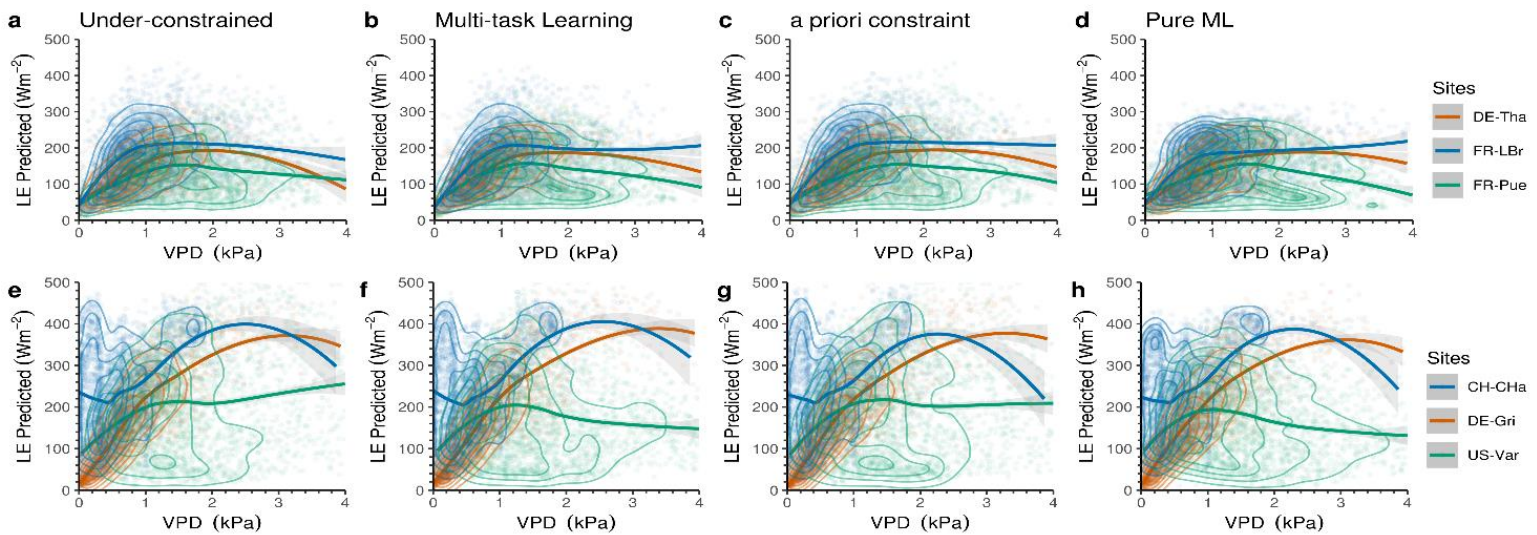


Figure 7: Evaluating Q_{LE} predictions against VPD for different models for forests (a-d) and grasslands (e-h). Higher evapotranspiration rates evident for grasslands compared to forests associated with higher stomatal conductance.

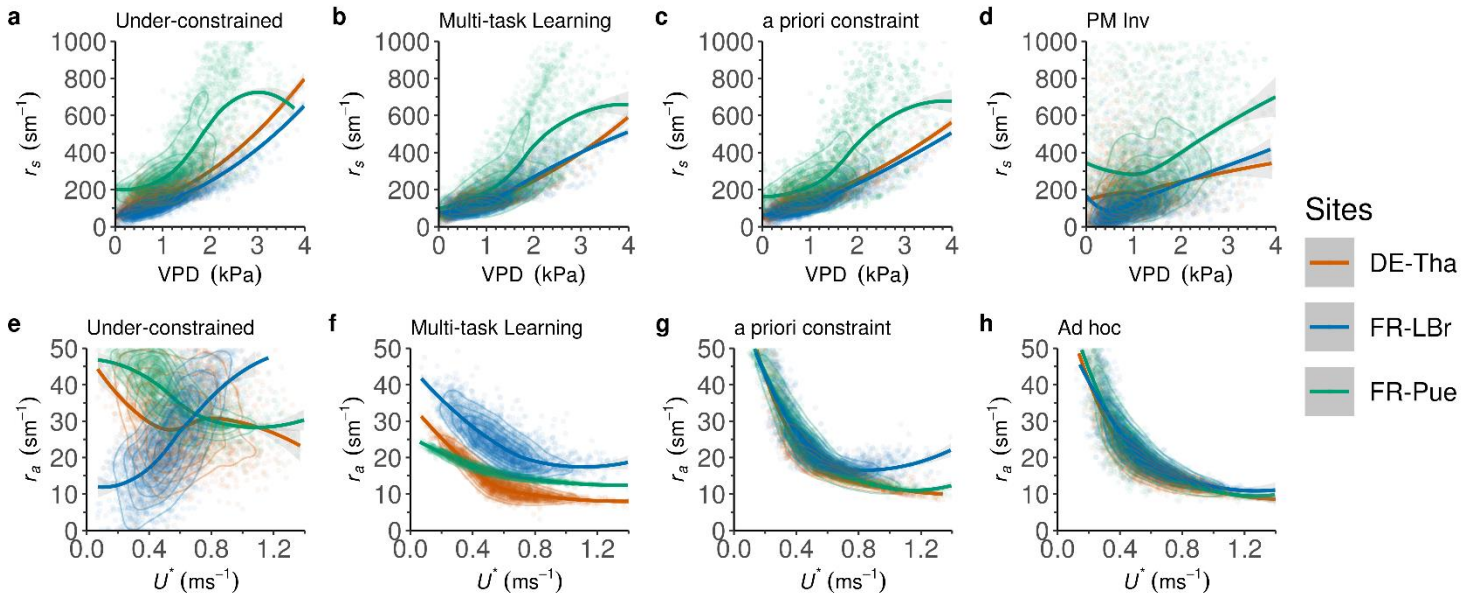
740

741

742

743

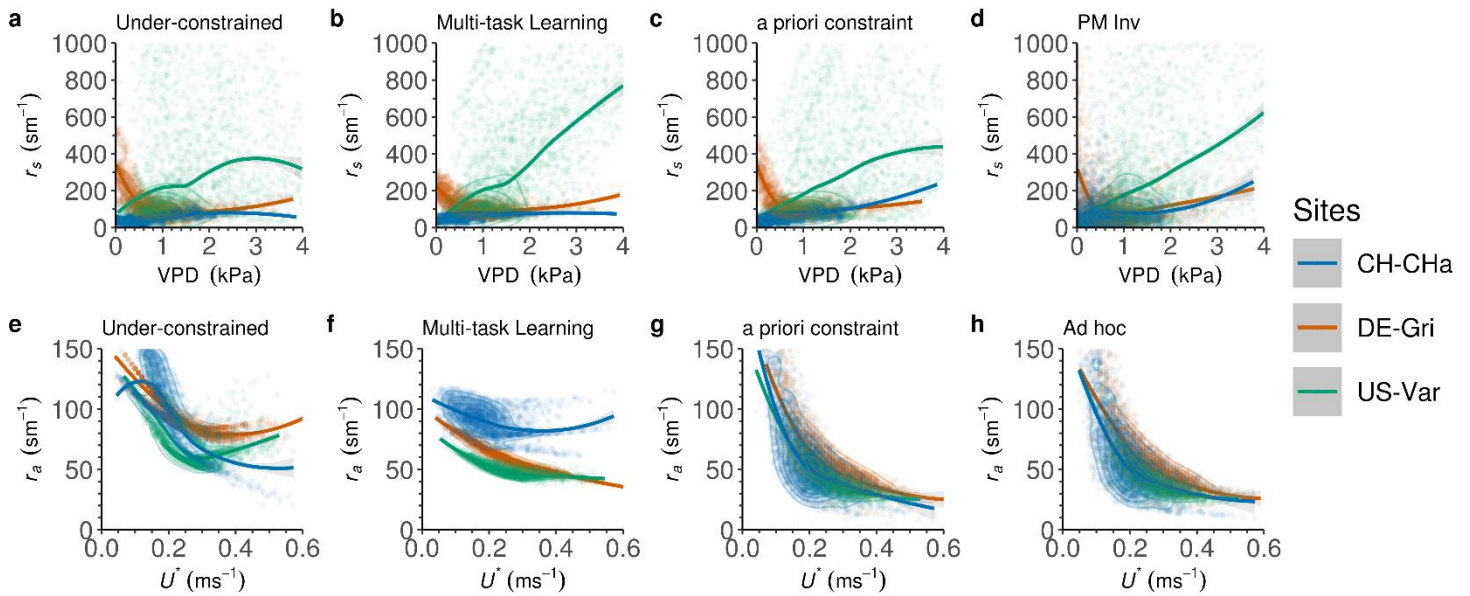
744



745

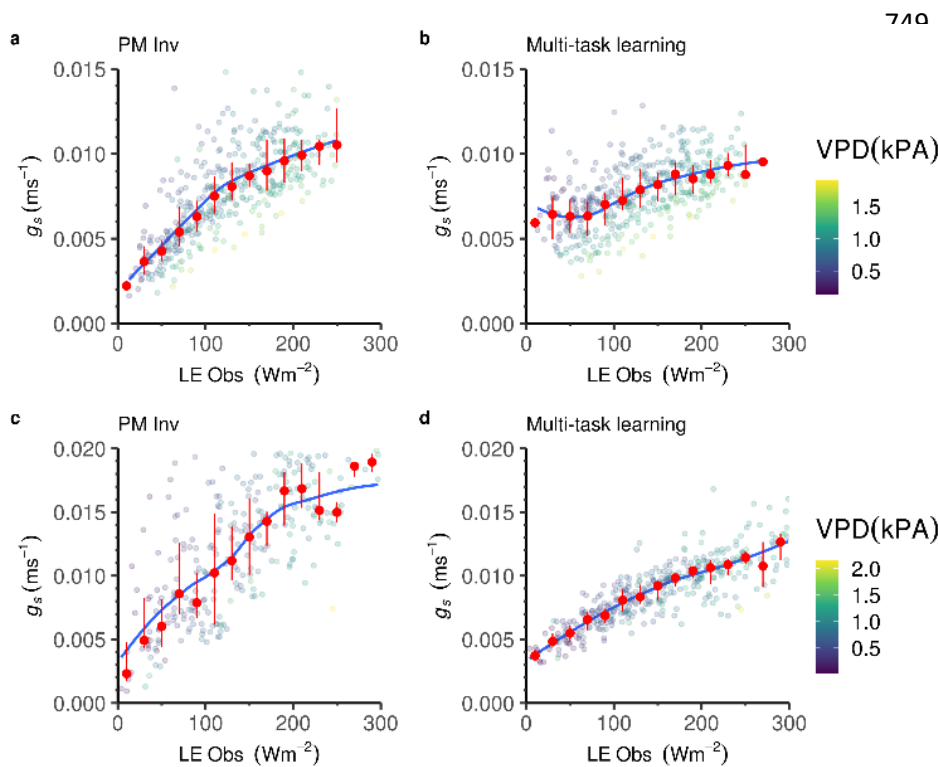
Figure 8: Assessing latent variables r_s and r_a against VPD and U^* respectively for different models in forests. Constrained hybrid models reveal physical consistency of latent variables compared to under-constrained model, especially under different environmental conditions.

746



747
 Figure 9: Assessing latent variables r_s and r_a against VPD and U^* respectively for different models in grasslands. The constrained hybrid models yield more physically consistent results compared to under-constrained model, and able to capture the vegetation and climate heterogeneities.

748



749
 Figure 10: Physical consistency of g_s and $Q_{LE_{obs}}$ with VPD at mean diurnal scale of DE-Tha forest (a,b) and DE-Gri grassland (c,d). The multi-task learning model is able to capture the same patterns as shown by Penman-Monteith, while being more resistant to noise in the data which may cause overestimation of surface conductance due to the instability of the inversion.